THE JOURNAL OF PHYSICAL CHEMISTRY B

Article

pubs.acs.org/JPCB

Computer Simulation of Fifth Generation Dendronized Polymers: Impact of Charge on Internal Organization

Oscar Bertran,*[,†] Baozhong Zhang,[‡] A. Dieter Schlüter,[‡] Martin Kröger,[‡] and Carlos Alemán*[,§,∥]

[†]Departament of Applied Physics, EEI, Universitat Politècnica de Catalunya, Pça Rei 15, Igualada 08700, Spain

[‡]Department of Materials, Institute of Polymers, Swiss Federal Institute of Technology, ETH Zurich, Wolfgang-Pauli-Str. 10, 8093 Zurich, Switzerland

[§]Departament of Chemical Engineering, ETSEIB, Universitat Politècnica de Catalunya, Diagonal 647, Barcelona E-08028, Spain

[∥]Centre for Research in Nano-Engineering, Universitat Politècnica de Catalunya, Edifici C′, C/Pasqual i Vila s/n, Barcelona E-08028, Spain

ABSTRACT: The internal organization of a fifth-generation dendronized polymer (PG5) has been investigated by atomistic molecular dynamics simulations in a vacuum. This study reveals an exceptional behavior of PG5 within the homologous series of *g*-generation PG*g* polymers. Three molecular configurations, which present a heterogeneous distribution of dendrons and an amount of backfolding lower than PG4 and PG6, have been obtained for PG5. The highest stability and closest agreement with available experimental data corresponds to a helical conformation characterized by a pitch of about 30 Å, thickness of 105 Å, and average density of 0.861 g/cm^3. While small angle neutron scattering studies of PG5 in solution show a constant radial density distribution around the backbone, we here in our vacuum studies find a cylindrical volume element of sharply reduced density reminiscent of a pore. This neutral PG5 was compared with its charged deprotected analogue, *de*PG5 in water, to see in as much the positive charges in the periphery of this macromolecule would affect its conformational behavior. During deprotection of PG5, the *tert*-butyloxycarbonyl protected amine groups are converted into ammonium, mimicking the experimental situation during a divergent synthesis procedure. The repulsive interactions among the positively charged ammonium groups are responsible for a huge (∼30%) reduction of the average density and a small (∼1%) increase of elongation of the helical backbone, which results in a structure with a spongy appearance. Also here, we find a reduced dendron density near the backbone which is compensated for by the pore being filled with water.

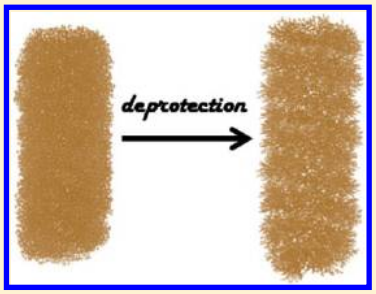

INTRODUCTION

Dendronized polymers (DPs) consist of regularly branched fragments (dendrons) densely attached along a linear polymer backbone. Steric repulsions among neighboring dendrons, increasing in strength with their generation number, *g*, compel polymer main chains to extend from random coils to weakly bent, rod-like cylinders typically found for DPs.[1−5] Accordingly, the rigidity, diameter, and properties of DPs can be tuned by varying *g*.[6] DPs represent an important class of single molecular nanomaterials with important potential applications, as for example in catalytic, drug delivery, and biosensors systems.[7−12]

On the other hand, atomistic modeling of the internal structure of DPs is a very challenging task[13−19] because of their huge dimensions and intrinsic conformational complexity, which reflect crowding and excluded volume interactions. Current computational facilities allow studies of these chemical systems, which were unaffordable a few years ago, enabling one to get microscopic information that often remains experimentally inaccessible. Within this context, we recently[19] used conformational search and growth procedures combined with molecular dynamics (MD) simulations to model the structure and properties of a homologous series of neutral DPs (Figure 1a), whose repeat units are regularly branched dendrons of generations *g* = 1−7, denoted PG1−PG7 (where PG*g* refers to a DP made of *g*-generation dendrons). The backbone of DPs with $g \leq 4$ was found to display an elongated shape (Figure 1b), while PG6 exhibited a helical conformation (Figure 1b). Furthermore, we predicted that the existence of defect-free DPs with $g \geq 7$ is precluded because of their stiffness and related strain onto their backbone. Both properties were seen to reflect packing constraints. Other calculated properties for these polymers were the fractal dimensionality, the local density profiles, the thickness, and the diffusion and load of small molecules inside DP structures. Experimental estimations,[6,20] when available, were in good agreement with theoretical predictions.

Despite the synthesis and structural properties of PG5 (Scheme 1) were recently reported,[21] this DP was excluded from our previous modeling study.[19] This was because preliminary simulations evidenced its seemingly exceptional behavior within the homologous series, indicating that the studies required for their thorough characterization are more extensive and elaborated for PG5 than for the other polymers of the series. Indeed, PG5 is the largest synthetic linear

Received: March 18, 2013
Revised: April 17, 2013
Published: May 6, 2013

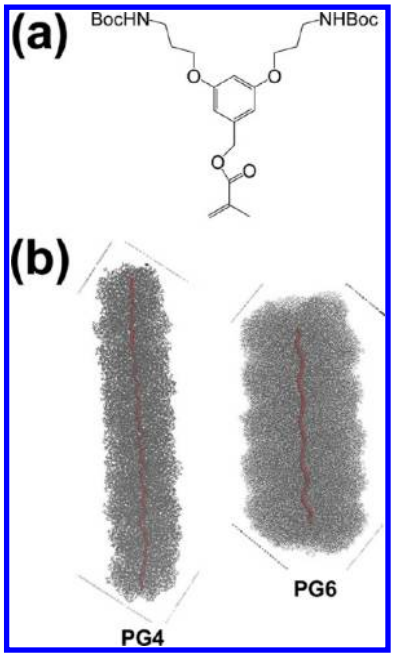

Figure 1. (a) Chemical structure of the monomer (branching unit) used for the synthesis of PGg. (b) Atomistic conformations provided in ref 18 for PG4 and PG6.

structure with molecular precision reported to date ($M \approx 200$ MDa), mimicking the thickness of some biological objects (e.g., microfilaments and cylindrical viruses). Structural studies on PG5, which were performed on solid substrates using different microscopy techniques, evidenced a change in the molecular shape with respect to PG2–PG4.[20,21] Specifically, the apparent height (h_{app}) of PG2, PG3, PG4, and PG5 adsorbed onto attractive mica substrate, which was measured by transmission electron microscopy (TEM), is 23, 34, 49, and 73 Å, respectively. Thus, the variation of the thickness, calculated as $\Delta h_{app} = h_{app}(g + 1) - h_{app}(g)$, is 11, 15, and 24 Å for PG3–PG2, PG4–PG3, and PG5–PG4, respectively, reflecting that the increment is significantly higher for the system with $g = 5$ than for the others at lower g.

In this work, we combine various computational strategies to determine the internal structure and properties of PG5. Results are going to be compared not only with available experimental measurements on PG5 but also with observations and predictions on PGg with $g \neq 5$. Furthermore, to examine the influence of the charges on the internal structure of DPs, the study has been extended to the deprotected PG5 (denoted as *de*-PG5, cf. Scheme 1). At the experimental level, deprotection is achieved by removing the *tert*-butyloxycarbonyl (Boc) protecting groups using trifluoroacetic acid.[6,21] Results evidence that removal of the Boc protecting groups from PG5 have a significant impact in the internal organization of the DP. Specifically, deprotection produces significant changes in the density and the backfolding (i.e., the looping phenomenon that describes the approach of the external branching units to the polymer backbone), which affect the thickness.

Scheme 1

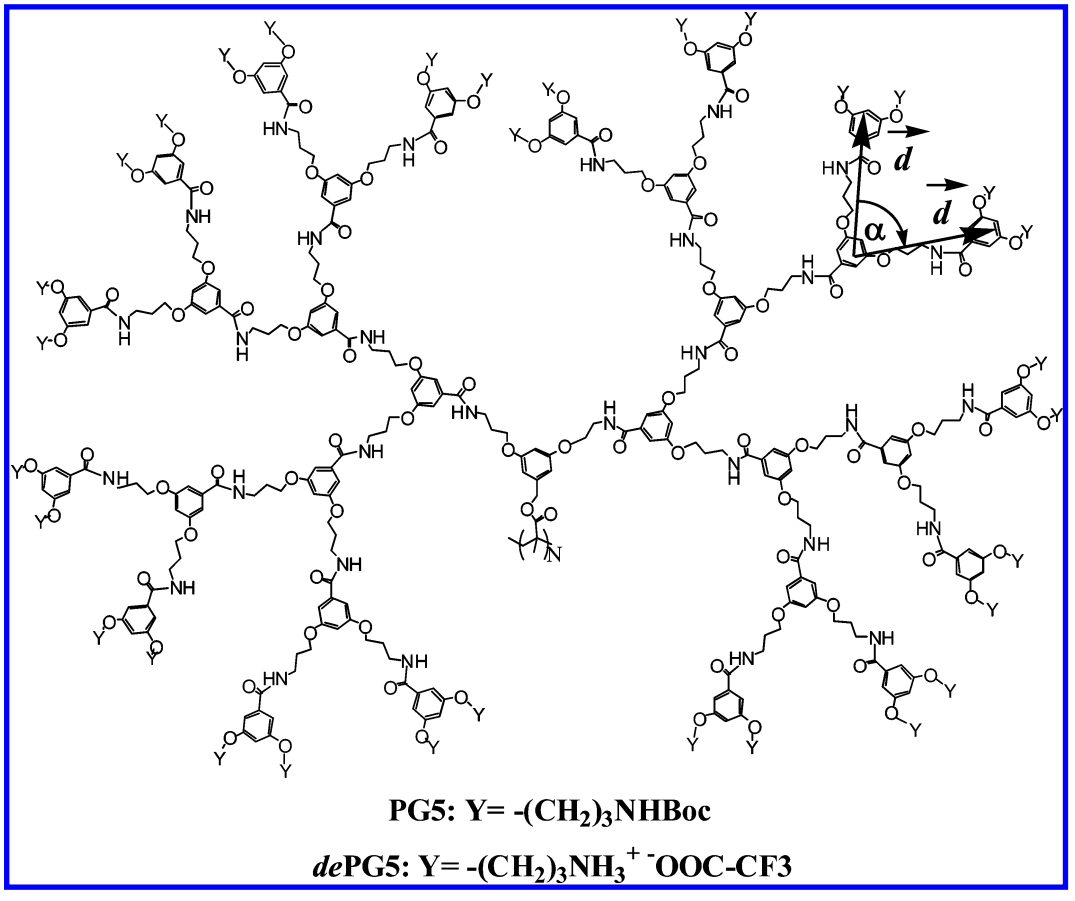

dx.doi.org/10.1021/jp402695g | J. Phys. Chem. B 2013, 117, 6007–6017

METHODS

Conformational Analysis. The conformational search and growth procedure already employed in our recent study for PG*g* with $g \neq 5$ consisted of a generation-by-generation growth process, which was applied following a bottom-up strategy.[19] This can be summarized as a multidimensional conformational analysis based on a reduced set of variables: (i) the backbone conformation, in which all the repeating units were assumed to be identical, and (ii) one virtual angle (θ) and one virtual dihedral (φ) defined to characterize the relative orientation between strands and branching units. Thus, 20 starting conformations, which resulted from the combination of five different backbone conformations with two values for θ and two for φ, were constructed for PG1.[19] Energy minimization of those without steric conflicts led to 16 homogeneous and regular structures, which were subsequently used to construct the 64 starting conformations of PG2 (i.e., combining them with the parameters θ and φ of the external layer: $16 \times 2 \times 2$).

Energy minimization of the 16 starting structures for PG2 produced five regular homogeneous and regular conformations,[19] with application of the growing procedure resulting in two and one conformations for PG3 and PG4, respectively. This bottom-up strategy has also been used in this work, even though some of the mentioned criteria have been modified because of the particular characteristics of PG5 (see next section). Specifically, homogeneity and regularity of a minimized conformation was defined by the two geometric parameters involving the outermost branching units (sometimes denoted "external dendrons") of a *g*-generation dendron: the vector between the first aromatic carbon of the corresponding branching unit and the center of masses of the *tert*-butyloxycarbonyl Boc groups (vector **d** of length *d*) and the angle (α) between the two vectors **d** for each external dendron (see Scheme 1). Minimized conformations were defined as "homogeneous and regular" when the distribution of α angles and backbone dihedral angles showed standard deviations below 20%. It should be noted that this criterion is biased to favor homogeneous arrangements at the outermost regions, since dendrons at the external layer are as numerous as the dendrons contained in all inner layers. An important consequence of the modification in the criteria used to define homogeneity and regularity is that recalculation of structures for PG1−PG4 with the new criteria became necessary. The structures that preserved regularity and homogeneity after minimization were submitted to 0.3 ns of MD at 298 K in a vacuum. Some enforced helical conformations lost the conformational regularity during this heating process, which enhanced the backbone strain. After this, the stability of the remaining structures was investigated in a vacuum in the "equilibration phase", which consists of simulations of 15 ns in a vacuum for each one.

Computational Details for PG5. Atomistic structures of PG5 were modeled in a vacuum considering a DP polymer chain with $N = 100$ repeat units. This solvent-free model corresponds to the situation encountered in the atomic force experiments.[21] Thus, both the large size of the polymer chain (i.e., 160902 explicit atoms) and the fact that structural information provided by experimental studies was obtained in a desolvated environment led us to perform the simulations in the absence of external forces. On the other hand, the rigidity of DPs, which prevents the existence of significant molecular distortions, and the lack of end-cap effects for systems larger than $N \approx 30$[19] indicate that a polymer chain with $N = 100$ should be considered as a representative model of realistic PG5.

Energy minimizations during pre-equilibration and MD simulations for the relaxation during the equilibration phase were performed with the NAMD program.[22] Minimization of the structures without overlapping was carried out using a conjugate gradient method. The energy was calculated using the AMBER force-field,[23] all the bonding and van der Waals parameters required for the DPs under study being taken from the generalized AMBER force-field (GAFF).[24] Atomic charges for the whole family of PG*g*, which were obtained using the restrained electrostatic potential (RESP) strategy,[25] were reported in our previous study.[19] Atom-pair distance cut-offs were applied at 12 Å to compute van der Waals and electrostatic interactions. Bond lengths involving hydrogen atoms were constrained using the SHAKE algorithm with a numerical integration step of 2 fs.[26]

MD simulations of a pre-equilibrated PG5 structure in a vacuum were performed by heating up the system from 0 to 298 K using a rate of 1 K each 1.5 ps. Coordinates of all the production ("relaxation") runs, which were 15 ns long, were saved every 5000 steps (10 ps intervals, 1500 snapshots for each model). Averages were obtained using the structures recorded during the last 10 ns of the simulation. The equilibration phase was generally followed by monitoring the system's energy, the end-to-end distance, and the radius of gyration.

Computational Modeling of *de*PG5. This charged system was modeled by constructing the starting geometries from the three models selected for PG5 (see next section). Simulations of *de*PG5 were carried out in aqueous solution, using explicit water molecules to represent the solvent. In order to keep the size of the system within affordable dimensions, the number of repeat units was reduced from $N = 100$ to $N = 75$. After this, the three PG5 models were transformed into the *de*PG5 ones by eliminating the protecting Boc groups of the amine functional groups from each external dendron, the resulting free amines being protonated to obtain positively charged ammonium groups at the end of the external layer. A trifluoroacetate anion ($^{-}O_2CCF_3$), which was used as a counterion, was positioned facing each ammonium group to provoke the electrical neutrality of the system.

A spherical solvent cap was defined around each of the three starting models, hereafter denoted ***de*PG5a**−***de*PG5c**, and filled with water molecules. The radii of the solvent caps were 110 (model ***de*PGa**), 130 (model ***de*PGb**), and 126 Å (model ***de*PGc**), which contained 95163, 210558, and 184553 water molecules, respectively. Accordingly, the total number of explicit atoms represented in these models was 422966, 769151, and 691136, respectively (i.e., including the 120677 atoms of the polymer chain and the 16800 atoms of the 2400 $^{-}O_2CCF_3$ molecules).

The force-field parameters of the charged dendrons and $^{-}O_2CCF_3$ counterions were taken from GAFF.[24] Atomic charges for *de*PG5 and counterions were obtained using RESP strategy.[25] Water molecules were represented by the TIP3P model of Jorgensen and co-workers.[27] As for PG5, simulations were carried out using the NAMD[22] software and the potential energy function of AMBER.[23] van der Waals interactions were calculated by applying an atom pair distance cutoff at 10 Å. Electrostatic interactions were extensively computed by means of Ewald summations. The real space term was defined by the van der Waals cutoff, while the reciprocal

dx.doi.org/10.1021/jp402695g | J. Phys. Chem. B 2013, 117, 6007−6017

space was computed by interpolation into an infinite grid of points (particle mesh Ewald) with the maximum space grid being 1.2 Å.[28]

Before running the production MD simulations, different consecutive rounds were performed to equilibrate and thermalize the system. First, water molecules were thermally relaxed by two consecutive runs, while the polymer chain was kept frozen during 0.5 ns of isothermal and 1.0 ns of isobaric relaxation. Hereafter, all atoms of the system were submitted to 1 ns of heating until the target temperature was reached (298 K), followed by 3 ns of thermal equilibration. Temperature was controlled by the weak coupling method,[29] using a time constant for the heat bath coupling of 1 ps. After this, the MD production run of each system at 298 K and 1 atm was 5 ns long. The numerical integration step was set to 2 fs, while the coordinates of the production run were saved every 5000 steps (500 snapshots for each model).

RESULTS AND DISCUSSION

Molecular Models for PG5. Utilization of the bottom-up strategy described in the Methods section, combined with the criteria used in our previous work to define "homogeneous and regular" conformations for PG1−PG4, led to a unique structure for PG5, hereafter denoted as **PG5a** (Figure 2). This structure

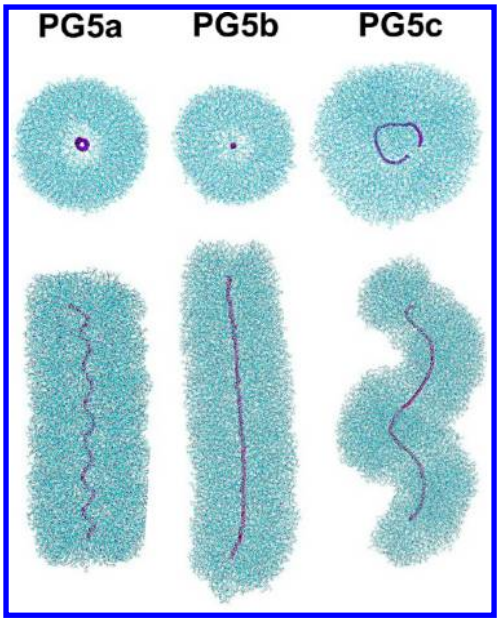

Figure 2. Atomistic conformations for **PG5a**, **PG5b**, and **PG5c** models in a vacuum. Two images are displayed for each model of PG5, which correspond to the equatorial projection of a section (top) and the axial (bottom) projection. All the structures were obtained after the 10 ns relaxation run.

consists of a helical backbone conformation that looks closer to the helix of PG6 than to the elongated conformation of PG4 (Figure 1b). However, the most striking feature of the **PG5a** model refers to the fact that internal and external dendrons adopt very different arrangements. This is clearly evidenced in Figure 3a, which compares the variation of the density as a function of radial distance r from the macromolecular backbone (MB) of **PG5a** with those of the models reported for PG4 and PG6. For this purpose, the macromolecular axis (MA) of DPs has been obtained from the coordinates of the atomistic backbone by linear regression, the MB coinciding with the MA

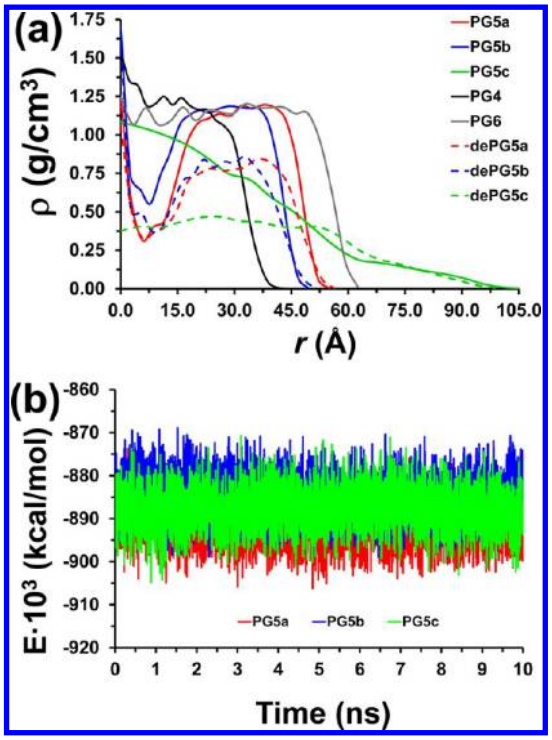

Figure 3. (a) Density profile for the PG5 and *de*PG5 models representing the density (ρ) against the distance to the backbone measured using the vector perpendicular to the helical axis (r). The profile displayed for each model corresponds to an average considering different cross sections within a given snapshot. Data were obtained by averaging over 1000 snapshots taken during the last 10 ns of the MD relaxation runs. Profiles for PG4 and PG6 (from ref 18) are included for comparison. (b) Temporal evolution of the potential energy along the last 10 ns of the relaxation MD runs for **PG5a**, **PG5b**, and **PG5c**.

over the extension of the atomistic backbone. Accordingly, the radial distances used to evaluate the density are the shortest distances to the atomistic backbone in a fashion that eliminates details on length scales comparable with an atomistic bond length.

Inspection of the profiles obtained for PG4 and PG6 indicates that the highest density is localized at the region close to the backbone, reaching values of 1.54 and 1.25 g/cm^3, respectively. After this, the density drops to 1.1−1.2 g/cm^3, remains constant over some range of distances, and finally decreases slowly and progressively until the external layer of the cylinder section has been reached. In contrast, the density of **PG5a** drops from 1.16 g/cm^3 at the backbone to 0.4−0.5 g/cm^3 still close to the backbone, and increases to 1.1−1.2 g/cm^3 at $r \approx 20$ Å. This density profile evidences a significant difference with respect to PG4 and PG6, which is consistent with a conformational variability at the branching units. Specifically, the low density region close to the backbone indicates that the conformation of dendrons within this region (made of internal dendrons) is different from that of dendrons closer to the external layer. The average α and d values for internal/external dendrons are 65°/79° and 9.42 Å/9.26 Å (i.e., α = 71°/77° and d = 9.40 Å/9.22 Å for PG4/PG6) This conformational variability results in a porous region located in the immediate neighborhood of the backbone (Figure 2). We find the existence of such a region to be peculiar for PG5, as it was clearly absent for all other PGg with $g \neq 5$.[19] It should be mentioned that small-angle neutron scattering (SANS) studies

dx.doi.org/10.1021/jp402695g | J. Phys. Chem. B 2013, 117, 6007−6017

in methanol solution suggested that no porous region is formed in PG5. However, the latter environment is significantly different from the solvent-free case examined in this work.[21]

In order to look for alternative structures without discontinuities at the radial density profile, the criterion used to define homogeneity and regularity was relaxed increasing from 20 to 40% the allowed standard deviation in the distribution of the α angles and backbone dihedral angles. Due to the generation-by-generation nature of the modeling strategy (see the Methods section), this change required additional simulations not only of PG5 but also of PG1−PG4, with the consequent increase of computational effort. Importantly, no qualitatively different arrangement was derived from the new simulations. The whole modeling process was furthermore repeated upon increasing the number of starting conformations, which was achieved by considering eight different backbone conformations. In addition to **PG5a**, another two new homogeneous and regular structures were obtained for PG5. Analysis of their atomistic representation, which is displayed in Figure 2, evidences their elongated (**PG5b**) and helical (**PG5c**) backbone conformation. Regarding to the latter, it is worth noting that **PG5a** and **PG5c** backbones differ in the internal diameter of the helix (i.e., the diameter defined by the backbone atoms), which is 5.9 and 30.0 Å, respectively. Thus, the backbone of **PG5c** defines a supramolecular helical structure with a twist angle (rotation per repeating unit) of h = 10.3° and a pitch (length of a complete helical turn) of L = 117 Å, while the geometric parameters for the secondary structure of **PG5a** are h = 25.7° and L = 30 Å.

The profiles of the density as a function of radial distance r from the MB for **PG5b** and **PG5c** are displayed in Figure 3a. As it can be seen, the profile of **PG5b** is very similar to that discussed above for **PG5a**, showing a heterogeneous distribution of the dendrons. Thus, the most remarkable differences correspond to the drops of density at the neighborhood of the backbone and at the external layer, which occur ∼5 Å before in **PG5b** due to the smaller diameter of the cylinder section. On the other hand, the profile calculated **PG5c** shows that the density drops slowly and progressively from the backbone, becoming practically zero (<0.1 g/cm^3) at $r \approx 85$ Å. It is worth noting that this particular profile is a consequence of the supramolecular structure of **PG5c**, whose axial projection does not resemble an ideal but a corrugated cylinder (i.e., the pitch of the helix is large enough to leave empty space between the local extremes of the projected width).

The radius of PG5 can be evaluated considering two different approaches based on the use of the density profiles displayed in Figure 3a. In the first one, which was also used for PG4 and PG6,[19] the radius was determined from the radial probability distribution profile, $p(r) \propto \rho(r)$. Considering that the density profile is approximately constant, for a homogeneous cylinder of yet unspecified radius $R^{(1)}$ (where the superindex 1 refers to the first approach) that satisfies $p(r) \approx 1/r^2$ subject to normalization, $\int_0^R p(r)\, dr^2$, with $dr^2 = 2r\, dr$, one has

$$\langle r^2 \rangle^{1/2} = \frac{R^{(1)}}{\sqrt{2}} \approx 0.71 \times R^{(1)} \quad (1)$$

In the second approach, the radius $R^{(2)}$ was estimated as the distance at which the radial density profile has dropped to half of its maximum value before reaching the external layer cylinder section. It should be noted that $R^{(1)}$ provides a good estimation for the visible thickness of **PG5a** and **PG5b** but overestimates the thickness of **PG5c**, while $R^{(2)}$ seems to underestimate the thicknesses of **PG5a** and **PG5b**. In the particular case of **PG5c**, the continuous drop of the density precludes a reliable estimation of the radius, even though $R^{(2)}$ is expected to be more reliable than $R^{(1)}$.

Table 1 compares the $R^{(1)}$ and $R^{(2)}$ values determined for the three models of PG5 with the half of the apparent height $(h/2)$

Table 1. Radius Assuming a Homogeneous Cylindrical Model, $R^{(1)}$, Radius Considering the Drop of the Density at the External Layer of the Model, $R^{(2)}$, Average Density, ρ_{av}, and Average Energy, $\langle E \rangle$, for the Investigated DPs[a]

	$R^{(1)}$ (Å)	$R^{(2)}$ (Å)	$(h/2)/R_{sol}$ (Å)	ρ_{av} (g/cm^3)	$\langle E \rangle$ (kcal/mol)
PG4	36.2		24.5[b]	1.07	
PG5a	52.5	42.0		0.861	−891319 ± 4592
PG5b	46.3	37.8	36.5[a]/∼50[c]	1.09	−885196 ± 4514
PG5c	73.2	∼62		0.23	−887642 ± 4699
PG6	58.7			1.11	
***de*PG5a**	52.7	42.2		0.57	−697962 ± 5186
***de*PG5b**	47.2	35.4		0.72	−681147 ± 5179
***de*PG5c**	79.3	55.0		0.21	−649060 ± 5287

[a]Data were obtained by analyzing the snapshots stored from MD simulations in a vacuum (PG*g*) and in aqueous solution (*de*PG5). The experimental estimates of the radius derived from TEM measurements of the height of DPs absorbed onto attractive mica $(h/2)$ and from SANS and cryo-TEM measurements in solution (R_{sol}) have been included (when available) for comparison. [b]Heights of PG*n* on mica determined by TEM (ref 19). [c]Radius determined in solution by SANS and cryo-TEM (ref 20).

of that DP absorbed onto attractive mica substrate, which was measured by transmission electron microscopy.[20] In our previous work on PG*g* with $g \neq 5$, we found that $R^{(1)}$ was systematically larger than $h/2$, which was attributed to the adsorption-induced flattening of the DP structures.[20] However, the variation of the difference $\Delta\tau = R_{gp} - h/2$ (where R_{gp} refers to the radius derived from MD simulations in ref 18) against g for g = 2, 3, and 4 was adjusted to an equation, $\Delta\tau = 0.25 \cdot e^{0.37 \cdot g}$ nm (R^2 = 0.973), able to describe both the influence of such a factor and the role of g in its relative importance (i.e., the degree of flattening decreases with increasing g).[19] Application of the latter equation to PG5 leads to $\Delta\tau$ = 1.59 nm, which is almost identical to the **PG5a** estimation (i.e., $R^{(1)} - h/2$ = 1.60 nm). On the other hand, the radius of PG5 in solution estimated by SANS and cryo-TEM, assuming a homogeneous density and a solvated polymer, was ∼50 Å by SANS and cryo-TEM.[21] This value was fully consistent with the width of the DP determined by SEM when freeze-dried (∼47 Å) and to the radius of a model cylinder (45.5 Å). It is worth noting that all these experimental measures are in excellent agreement with the $R^{(1)}$ value predicted for the **PG5a** model (i.e., 52.5 Å). The different predictions and experimental estimations of the radius discussed above for the homologous series of PG*g* polymers are represented in Figure 4.

The average densities (ρ_{av}) evaluated from the density profiles displayed in Figure 3a, $\rho_{av} = \sum_i \rho_i \Delta(r_i^2)/R^2$ (where $R = R^{(1)}$ for **PG5a** and **PG5b** and $R = R^{(2)}$ for **PG5c**), are included in Table 1. The ρ_{av} values predicted in our previous work ranged from 0.97 g/cm^3 for PG1 to 1.11 g/cm^3 for PG6,[19] while experimental measurements for solutions of dendron units in dimethylformamide and dichlorobenzene led to values of 1.10 g/cm^3.[20] The ρ_{av} calculated for **PG5a** and **PG5b** (0.86

dx.doi.org/10.1021/jp402695g | J. Phys. Chem. B 2013, 117, 6007−6017

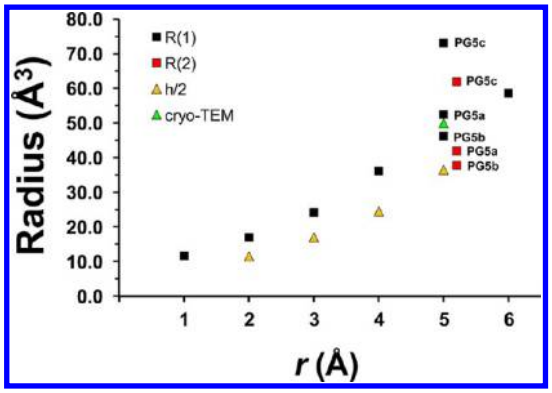

Figure 4. Graphical representation of $R^{(1)}$, $R^{(2)}$, $h/2$, and cryo-TEM radius versus g. $h/2$ and cryo-TEM radius were taken from ref 19.

and 1.09 g/cm^3, respectively) are close to these values, especially for the latter, whereas a significantly lower value has been obtained for **PG5c** (0.23 g/cm^3) due to its unique supramolecular structure.

Figure 3b represents the temporal evolution of the potential energy along the last 10 ns of the relaxation MD runs for **PG5a**, **PG5b**, and **PG5c**. The potential energy remains constant along the whole trajectory, evidencing the stability of the three structures. The averaged potential energies, which were calculated using the last 10 ns of the simulations, are displayed in Table 1. Although the three values were relatively similar, the results suggest that the structure with the elongated backbone is the least stable while the helical structure with a porous region close to the backbone (**PG5a**) provides the most stable interactions.

Analysis of the Backfolding. The particularities of the PG5 models with respect to those of PGg with higher or lower g should be attributed to the length of the dendron, which affects the backfolding of the external dendrons. This phenomenon, which is provoked by the unique architecture of DPs, consists of the approximation of the external dendron to the backbone and increases with g. In order to investigate the backfolding in PG5, both the radial probability distribution of the Boc end groups ($g_{Boc\text{-}b}$) and the number of the aromatic carbon atoms normalized with respect to the number of repeat units (N_{Car}/N, where $N = 100$) as a function of the distance (r) to the MB have been calculated for **PG5a**–**PG5c**, with the resulting profiles being compared with those obtained for PG4 and PG6 in Figure 5.

The $g_{Boc\text{-}b}$ profile obtained for PG6 showed a peak centered at r = 57 Å and a broad tail decaying to shorter distances (Figure 4a), indicating a significant number of Boc groups at a distance close to the backbone.[19] This distribution was also identified for PG4 with a peak at r = 35 Å, whereas for PG1–PG3 the size of the inner tails decreased with g and the profiles became pseudosymmetric.[19] Moreover, the peak is higher for PG4 than for PG6, indicating that the backfolding is more abundant in the latter than in the former. Figure 6 includes a detailed view of a representative dendron for PG4 and PG6, which reflects at the molecular level the information provided by the $g_{Boc\text{-}b}$ profiles. Furthermore, Figure 6 reveals some important differences in the backfolding at the region near the backbone. Thus, some external dendrons of PG4 tend to be located at the inner region. However, some external dendrons of PG6 not only occupy the inner region but are also located in the region immediately next to the backbone, inducing local

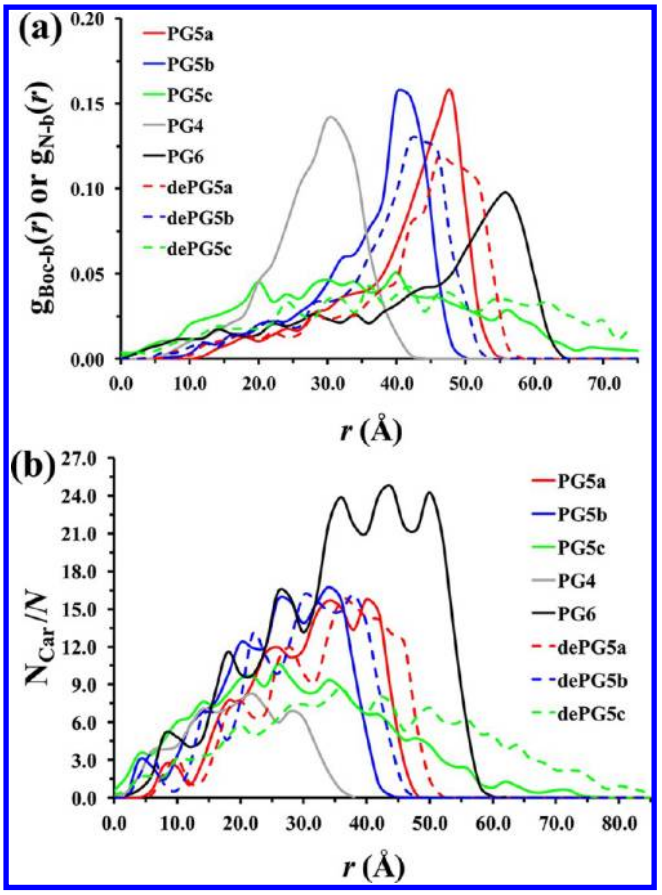

Figure 5. (a) Radial distribution function of the dendrons of the external layer for PG5 and *de*PEG5 models measured through the end Boc ($g_{Boc\text{-}b}$) and ammonium ($g_{N\text{-}b}$) groups, respectively. (b) Number of aromatic carbon atoms per repeating unit (N_{Car}/N) as a function of the distance from the backbone for PG5 and *de*PEG5 models. Profiles displayed for each model correspond to the average over 1000 snapshots taken during the last 10 ns of relaxation runs. Profiles for PG4 and PG6, which were calculated using the snapshots from simulations described in ref 18, are included for comparison.

conformational strain (i.e., the backbone is compressed by the surrounding effect of these closest external dendrons). Indeed, the elongated-to-helical transition observed when g increases from 4 to 6 (Figure 1) was attributed to the fact that the backfolding-induced strain is significantly relieved when the elongated backbone transforms into the helical one.

The shape of the $g_{Boc\text{-}b}$ profiles calculated for **PG5a** and **PG5b** resembles those of PG4 and PG6, with a peak centered at r = 46 and 40 Å, respectively, and a tail decaying to shorter distances. However, detailed inspection reveals a significant difference, which consists of the complete absence of Boc groups at distances shorter than 12 (**PG5a**) and 8 Å (**PG5b**). Thus, the approximation of the external dendrons to the backbone helical axis is smaller for these PG5 models than for PG4 and PG6. This is because PG5 side chains are not long enough to provoke a complete backbone wrapping phenomenon, as in PG6, and are too bulky and rigid to allow the approximation degree found in PG4. Accordingly, the behavior of **PG5a** and **PG5b** should be actually considered as intermediate between those of PG6 and PG4 but with the conformational restrictions (i.e., rigidity and size) associated with g = 5. Although the backfolding of **PG5c** is apparently higher than that of PG6, Figure 6 clearly proves that it is similar

dx.doi.org/10.1021/jp402695g | J. Phys. Chem. B 2013, 117, 6007–6017

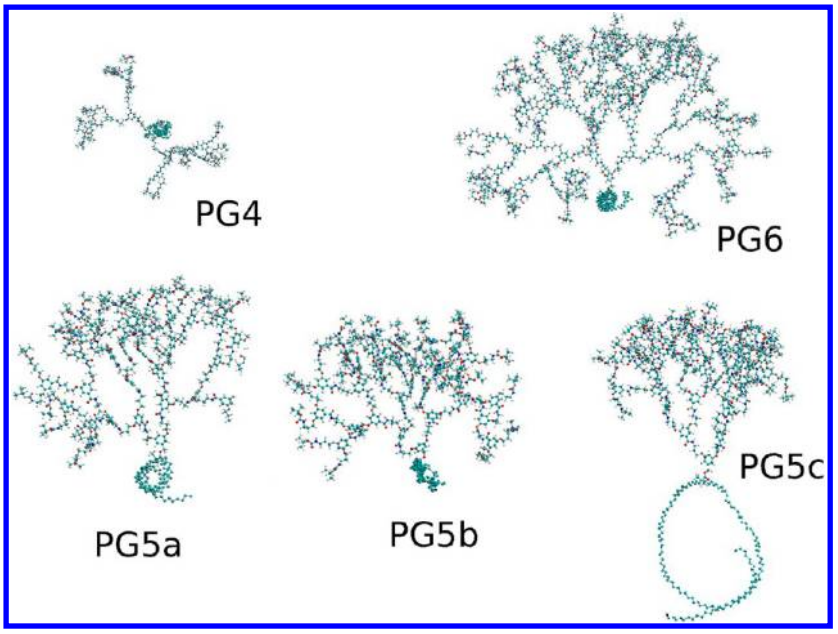

Figure 6. Detailed views of a representative dendron of PG4, PG6, **PG5a**, **PG5b**, and **PG5c** after complete relaxation using 15 ns of MD. The two views clearly show that the amount of backfolding depends on both the generation g and the backbone conformation.

to that of **PG5a** and **PG5b**. Thus, the unrealistic impression given in Figure 5a for **PG5c** is due to the particular width of the helical backbone conformation.

All of these features are corroborated by the profiles showing the distribution of the number of total aromatic carbon atoms per repeat unit (N_{Car}/N) as a function of r, which are displayed in Figure 5b. The number of aromatic carbon atoms per repeat unit is 90, 186, and 378 for PG4, PG5, and PG6, respectively. Inspection of the variation of N_{Car}/N as a function of r indicated that ∼50% of the aromatic atoms of PG4 and PG6 are located at r < 20 and 37 Å, respectively. For **PG5a**, **PG5b**, and **PG5c**, the distance required to get the same distribution is 31, 30, and 37 Å, respectively. On the other hand, the 90 aromatic carbons of each repeat unit of PG4 are located at r < 37 Å, whereas the number of aromatic carbons comprised in the same space grows to 97, 131, 120, and 190 for **PG5a** (∼48%), **PG5b** (∼70%), **PG5c** (∼64%), and PG6 (∼50%), respectively. Considering the radii of such structures (see Table 1), these distributions reflect that the backfolding is less pronounced in PG5 (especially **PG5a**) than in PG4 and PG6.

Molecular Models for *de*PG5. Starting geometries for the ***de*PG5a**, ***de*PG5b**, and ***de*PG5c** models were constructed applying the procedure described in the Methods section to the last snapshot recorded from the production MD simulations of **PG5a**, **PG5b**, and **PG5c**, respectively. After minimization and thermalization, production MD runs were performed considering a spherical water cap centered on each model. Figure 7 represents a complete view of the final atomistic models obtained for ***de*PG5a**, ***de*PG5b**, and ***de*PG5c** at the end of the subsequent MD equilibration phase. As it can be seen, the backbone conformation shown by the models of the deprotected DPs is very similar to those of the protected ones, even though all the structures become more elongated. Thus, the average internal diameters of the ***de*PG5a** and ***de*PG5c** helices is 7.0 and 39.1 Å, respectively, while the average length of the elongated backbone conformation found for ***de*PG5b** is 2.6 Å per repeat unit (i.e., the average length for **PG5b** is 2.4 Å per repeat unit). In addition, comparison of

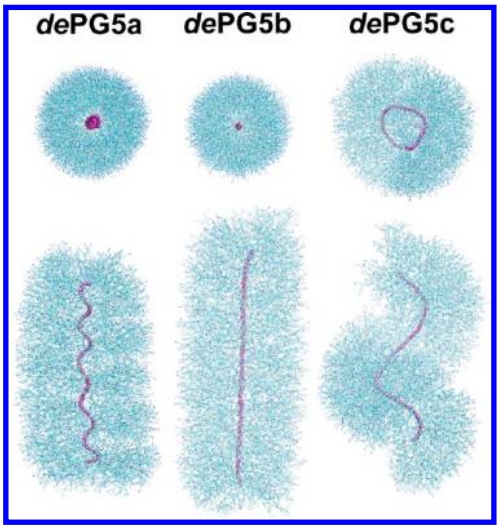

Figure 7. Atomistic conformations for ***de*PG5a**, ***de*PG5b**, and ***de*PG5c** models in aqueous solution. Two images are displayed for each model of *de*PG5, which correspond to the equatorial (top) and axial (bottom) projections. All the structures were obtained after the 5 ns relaxation run. Water molecules have been removed for clarity.

Figures 2 and 7 reveals a significant difference between the models calculated for *de*PG5 and PG5: the structures obtained for the deprotected DP are much more "*spongy*" than those achieved for the protected one. Moreover, such sponginess is expected to be accompanied by a significant reduction in the density.

Figure 3a includes the variation of the density as a function of radial distance r from the MB of ***de*PG5a**–***de*PG5c**. Amazingly, the shape of the profiles is practically identical for the *de*PG5 and PG5 models, even though the density is clearly smaller for the former than for the latter. For example, after the initial decay to 0.4–0.5 g/cm^3 at the region nearest to the backbone, the density of ***de*PG5a** and ***de*PG5b** increases to 0.7–0.8 g/cm^3 rather to 1.1–1.2 g/cm^3, as was observed for **PG5a** and **PG5b**. Similarly, the density of ***de*PG5c** remains approximately

dx.doi.org/10.1021/jp402695g | J. Phys. Chem. B 2013, 117, 6007–6017

constant from the backbone to $r \approx 55$ Å at ~0.4 g/cm^{-3}, this value being smaller than that obtained for **PG5c** in the same region. The reduction in the density caused by deprotection is also very apparent in the ρ_{av} values listed in Table 1. Thus, deprotection produces a decrease of the density that ranges from 10% (***de*PG5c**) to 33−34% (***de*PG5a** and ***de*PG5b**).

Table 1 includes the $R^{(1)}$ and $R^{(2)}$ values for three calculated models of *de*PG5. As it can be seen, the resulting values are very similar to those obtained for PG5, with $\Delta R^{(1)} = R^{(1)}_{dePG5} - R^{(1)}_{PG5}$ being 0.2 and 0.9 Å for (***de*)PG5a** and (***de*)PG5b**, respectively, and $\Delta R^{(2)}$ being ~−8 Å for (***de*)PG5c**. This feature suggests that the decrease of the density in *de*PG5 and, therefore, the spongy aspect of *de*PG5 models are due to reduction of the backfolding. In order to corroborate this feature, the radial probability distribution function of the end ammonium groups ($g_{N\text{-}bb}$) as a function of the distance (r) to the MB have been calculated for ***de*PG5a**−***de*PG5c** models. It is worth noting that the $g_{N\text{-}b}$ profiles, which are included in Figure 5a, are directly comparable to the $g_{Boc\text{-}b}$ profiles calculated for **PG5a**−**PG5c**. For all models, the backfolding was clearly lower for the deprotected DP than for the protected one. This feature is especially remarkable for **PG5a** and ***de*PG5a** models, since **PG5a** showed the closest similarity with experimental information and, in addition, was the most stable PG5 model. Thus, although such two models showed a peak centered at r = 47 Å, integration of the broad tails decaying to shorter distances evidenced that backfolding is around 32% smaller for ***de*PG5a** than for **PG5a**. The same feature is reflected in Figure 5b, which compares the number of the aromatic carbon atoms normalized with respect to the number of repeat units (N_{Car}/N, where N = 100) as a function of the distance (r) to the MB for ***de*PG5a**−***de*PG5c** and **PG5a**−**PG5c**. The reduction in the backfolding upon deproctection has been attributed to the electrostatic repulsions generated by the ammonium end groups, which limit the interpenetration of the dendrons around the backbone.

The number of water molecules located inside the DP was evaluated by considering an imaginary cylinder defined by a radius that is 0.85·$R^{(1)}$ (***de*PG5a** and ***de*PG5b**) or 0.85·$R^{(2)}$ (***de*PG5c**) and the length corresponding to 40 repeat units. Inspection of the number of water molecules contained in such a cylinder allowed us to conclude that the average number of water molecules inside the *de*PG5 hydrophobic interior is 120, 107, and 270 per repeat unit for ***de*PG5a**, ***de*PG5b**, and ***de*PG5c**, respectively. Figure 8 represents the water density as a function of radial distance r from the MB for the three *de*PG5 models. As it can be seen, the profiles of ***de*PG5a** and ***de*PG5b** show a broad peak at the internal region, reflecting the presence of water inside the dendron. Comparison with Figure 3a indicates that water molecules inside the DP compensate the reduction of the dendron density at the region near the backbone. Water molecules filling the pore of ***de*PG5a** and ***de*PG5b** are depicted in Figure 9, which displays a cross section of the structures obtained after the 5 ns relaxation runs. Because of its particular shape, analysis of the water molecules inside ***de*PG5c** (Figure 9) is more ambiguous than that for ***de*PG5a** and ***de*PG5b**.

The specific interactions formed between *de*PG5 and such water molecules have been found to be both N−H···OW and O···HW−OW hydrogen bonds, where N−H and O refer to the atoms in the amide groups of the deprotected DP while HW and OW refer to atoms belonging to water molecules. Parts a and b of Figure 10 display the partial radial distribution

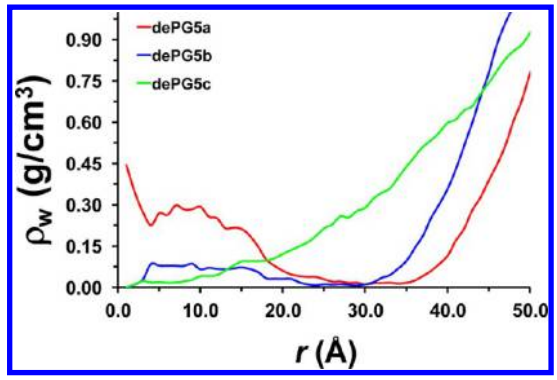

Figure 8. Density profile for the *de*PG5 models representing the water density (ρ_w) against the distance to the backbone measured using the vector perpendicular to the helical axis (r). The profile displayed for each model corresponds to an average considering different cross sections within a given snapshot. Data were obtained by averaging over 1000 snapshots taken during the last 5 ns of the MD relaxation runs.

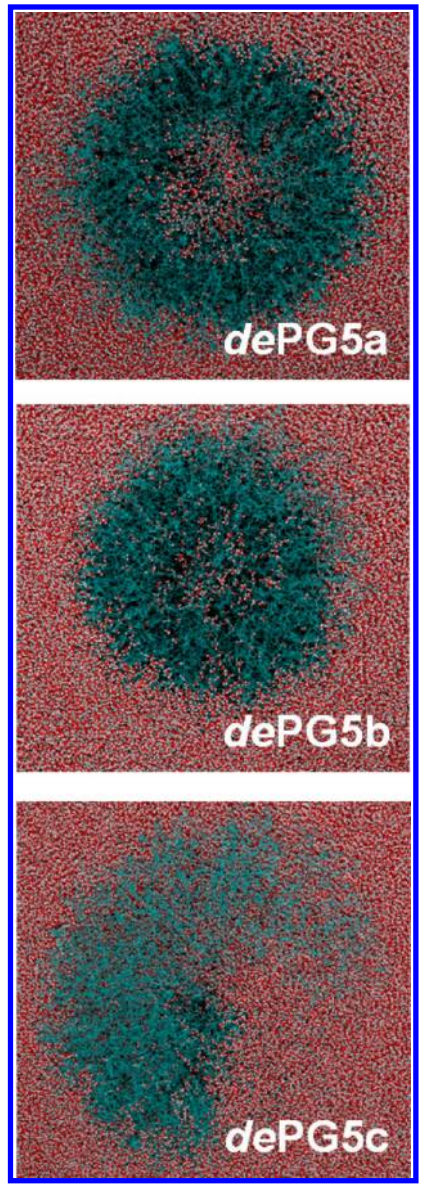

Figure 9. Cross section of the ***de*PG5a**, ***de*PG5b**, and ***de*PG5c** models in aqueous solution showing the water molecules inside the DP.

dx.doi.org/10.1021/jp402695g | *J. Phys. Chem. B* 2013, 117, 6007−6017

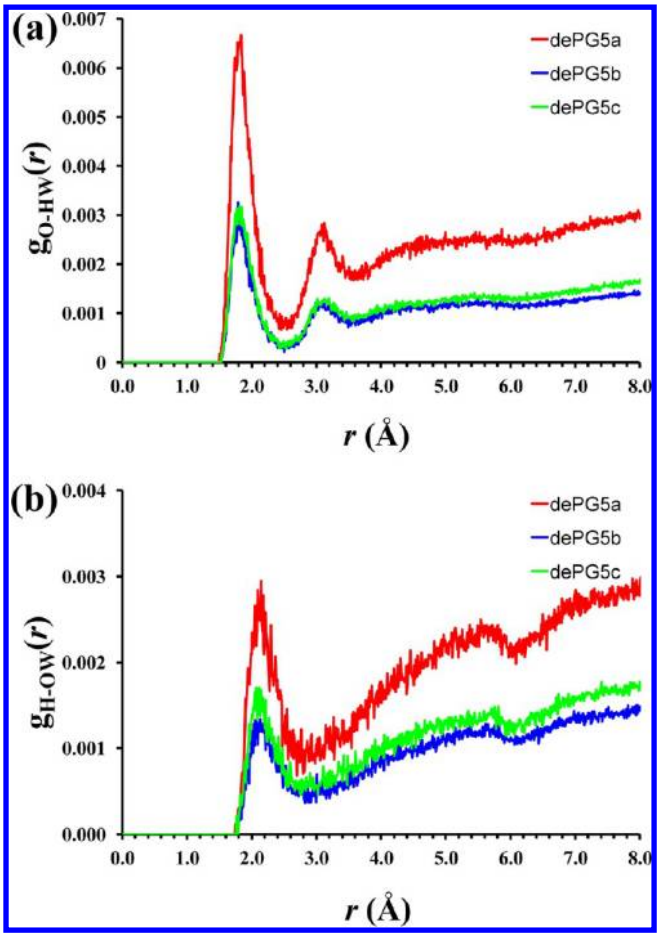

Figure 10. Partial distribution functions for (a) O···HW and (b) H···OW pairs in ***de*PG5a**, ***de*PG5b**, and ***de*PG5c** models.

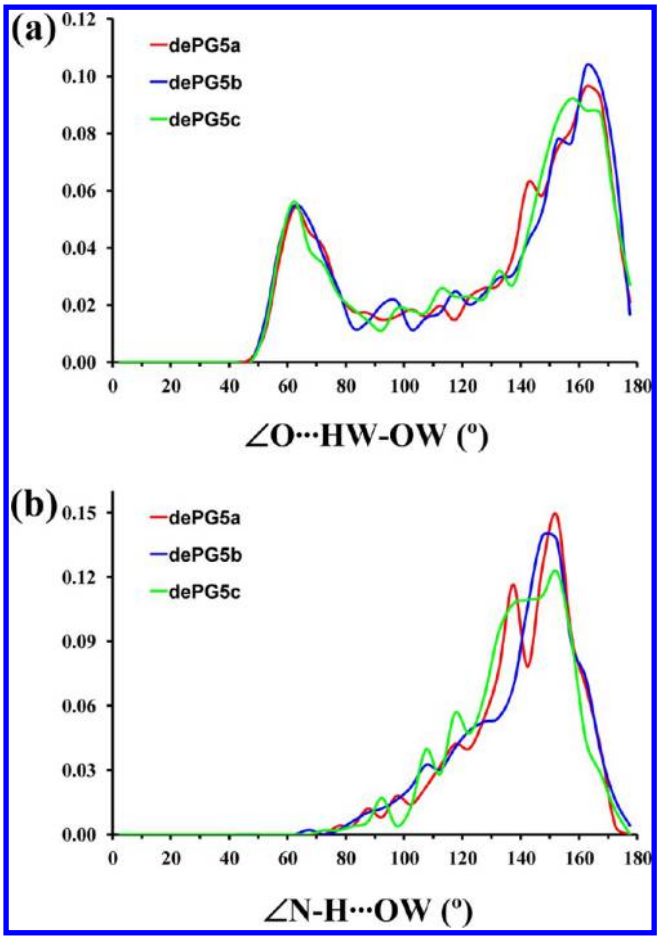

Figure 11. Distribution of the (a) ∠O···HW−OW and (b) ∠N−H···OW angles in the corresponding hydrogen bonds for ***de*PG5a**, ***de*PG5b**, and ***de*PG5c** models.

function of O···HW (g_{O-HW}) and H···OW (g_{H-OW}) pairs, respectively. As it can be seen, O···HW−OW hydrogen bonds are the most abundant, with the profiles of the three models showing a high and narrow peak centered at a distance of 1.825−1.845 Å (Figure 10a). This value is practically identical to that typically found for conventional H···O hydrogen bonds.[30] Moreover, a second peak centered at 3.075−3.145 Å is detected in the g_{O-HW} functions of ***de*PG5a**−***de*PG5c**. The latter peak is consistent with the formation of small water clusters around the amide groups of the DP. A similar clustering organization was recently reported for water molecules absorbed by a polyaniline emeraldine base,[29] in which water molecules form hydrogen bonds with the amine and, especially, the imine nitrogen atoms of polyaniline. The g_{H-OW} profiles displayed in Figure 10b show a peak centered at 2.115−2.145 Å, indicating that, independently of the model, the hydrogen bonding distance is ∼0.3 Å larger for the N−H···OW interactions than for the O···HW−OW ones. Furthermore, no other clear peak is detected at higher distances, indicating that the formation of well-defined clusters is much less frequent in the former than in the latter hydrogen bonds.

Parts a and b of Figure 11 display the distribution of the ∠O···HW−OW and ∠N−H···OW angles, respectively, in the corresponding hydrogen bonds. For this purpose, all the interactions with O···HW or H···OW distances lower than 3.0 Å have been considered for the evaluation of the hydrogen bonding angles. The profiles for the ∠O···HW−OW angles show two peaks in all cases. The most populated, which is centered at 157−167°, is consistent with the hydrogen bonding angles typically found for conventional interactions. The second peak, which is centered at 62−65°, must be attributed to water molecules comprised within the cluster mentioned above but not directly interacting with the C═O moieties of *de*PG5. Thus, although the cutoff used to select hydrogen bonds was large enough to include all O···HW−OW hydrogen bonds, some water molecules belonging to the second hydration shell (i.e., the cluster) were also allowed to enter within the set of examined interactions. In any case, it should be noted that the second peak is well-defined, indicating that the clusters adopt ordered organizations with a common pattern. The distributions displayed in Figure 11b indicate that ∠N−H···OW angles usually range from 135 to 165°, independently of the model. No other peak was obtained in these cases, which is consistent with absence of cluster obtained from Figure 10b.

The local strain at the backbone provoked by deprotection of PG5 has been estimated by measuring the average bond length between two consecutive carbon atoms belonging to the backbone. The values obtained for the **PG5a**, **PG5b**, and **PG5c** models are 1.552 ± 0.029, 1.555 ± 0.031, and 1.577 ± 0.034 Å, respectively, which are very close to the equilibrium value of the GAFF force-field (1.550 Å). The C−C bond length increases to 1.572 ± 0.035, 1.565 ± 0.036, and 1.615 ± 0.038 Å for the ***de*PG5a**, ***de*PG5b**, and ***de*PG5c** models, respectively. These increments indicate that local strain increases upon deprotection, though in a very slight way, especially for the two

dx.doi.org/10.1021/jp402695g | J. Phys. Chem. B 2013, 117, 6007−6017

former models. Indeed, it should be noted that the lowest strain was obtained for **PG5a** and ***de*PG5a**.

The potential energies of the ***de*PG5a**–***de*PG5c** models remained constant during the last 5 ns of dynamical relaxation (not shown), as occurred for **PG5a**–**PG5c** (Figure 3c). Inspection of the energies averaged during such a period of the trajectories (Table 1) indicates that ***de*PG5a** is the most stable. This result is fully consistent with the highest stability of the **PG5a** model, especially considering that *de*PG5 was experimentally derived from the deprotection of PG5 with neat trifluoroacetic acid rather than by reaction of *de*PG4 with an active deprotected dendron. Accordingly, the conversion of PG5 into *de*PG5 cannot induce significant changes in the backbone and the internal dendrons, which are constrained to stay at the adopted conformation because of both the lack of space induced by the complex architecture of DPs. The conformational similarity and highest stability of the ***de*PG5a** and **PG5a** models allow us to explain consistently the organization of the two fifth-generation macromolecules at the atomistic level.

Summary. The results discussed in the above sections indicate that **PG5a** and ***de*PG5a** are the most appropriate models for PG5 and *de*PG5, respectively. These models are not only the most stable but also the most consistent with available experimental data and theoretical predictions previously reported for PG*g* with $g \neq 5$. Specifically, the radius predicted for **PG5a** almost matches the values obtained in solution by SANS and cryo-TEM.[21] Moreover, this model is consistent with the transition from the elongated structure predicted for PG1–PG4 to the homogeneous helical one obtained for PG6.[19] **PG5a** exhibits a helical backbone that resembles PG6 but with a heterogeneous distribution of the atoms, which produces a drop of the local density in the region around the backbone. In addition, the radius of **PG5a** perfectly fits into the equation derived from PG1–PG4 models to adjust the predicted radius with the half of the apparent height determined by TEM.[19]

On the other hand, ***de*PG5a** has been derived from **PG5a**, which is fully consequent with the fact that *de*PG5 is experimentally produced by deprotecting PG5 and, therefore, no significant conformational arrangement is expected. Specifically, elimination of the Boc groups and protonation of the free amine only results in an elongation of the **PG5a** helix and a reduction of the backfolding. These changes, which are reflected in the superposed structures displayed in Figure 12, are induced by strong repulsive interactions among the positively charged ammonium groups. As a result, the density decreases upon deprotection, resulting in a structure with a spongy appearance.

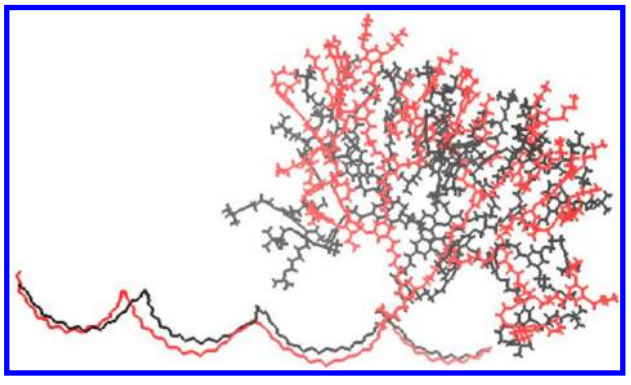

Figure 12. Superposition of a representative dendron of **PG5a** (black) and ***de*PG5a** (red) models for PG5 and *de*PG5, respectively.

CONCLUSIONS

The structure of the fifth-generation DP has been modeled using MD simulations, both Boc-protected and deprotected charged side groups being considered. After examination of different models, the structures showing a helical backbone conformation with an internal diameter of 5.9 (PG5) and 7.0 Å (*de*PG5) are found to be the most stable and the most consistent with previous experimental and theoretical studies. An important insight from these models is the heterogeneous distribution of the atoms, which leads to a region with low density (pore) surrounding the backbone. The particular radial density distributions of PG5 and *de*PG5 are consequences of the size of the side groups, which are large enough to promote backbone transition from the elongated conformation of PG*g* with $g \leq 4$ to the helix but too short to enable the significant degree of backfolding found for PG6.

Elimination of the Boc protecting groups and protonation of the free amines results in structural changes, even though the main characteristics of the model (e.g., helical backbone, heterogeneous density distribution, and limited backfolding) are preserved. Specifically, *de*PG5 exhibits an elongated helical backbone, a reduced density, and a reduced amount of backfolding as compared to PG5. The combination of these changes reflecting repulsive interactions between the positively charged ammonium groups leads to a structure with a spongy-like appearance.

AUTHOR INFORMATION

Corresponding Author

*E-mail: oscar.bertran@upc.edu (O.B.); carlos.aleman@upc.edu (C.A.).

Notes

The authors declare no competing financial interest.

ACKNOWLEDGMENTS

Financial support from the MICINN and FEDER (MAT2012-34498) and Generalitat de Catalunya (research group 2009 SGR 925 and XRQTC) is gratefully acknowledged. Support for the research of C.A. was received through the prize "ICREA Academia" for excellence in research funded by the Generalitat de Catalunya. Authors are indebted to the Centre de Supercomputació de Catalunya (CESCA) for the computational resources provided.

REFERENCES

(1) Zhang, A.; Shu, L.; Bo, Z.; Schlüter, A. D. Dendronized Polymers: Recent Progress in Synthesis. *Macromol. Chem. Phys.* **2003**, *204*, 328–339.

(2) Percec, V.; Ahn, C.-H.; Cho, W.-D.; Jamieson, A. M.; Kim, J.; Leman, T.; Schmidt, M.; Gerle, M.; Möller, M.; Prokhorova, S. A.; et al. Visualizable Cylindrical Macromolecules with Controlled Stiffness from Backbones Containing Libraries of Self-Assembling Dendritic Side Groups. *J. Am. Chem. Soc.* **1998**, *120*, 8619–8631.

(3) Yoshida, M.; Fresco, Z. M.; Ohnishi, S.; Fréchet, J. M. J. Efficient Divergent Synthesis of Dendronized Polymers with Extremely High Molecular Weight: Structural Characterization by SEC-MALLS and SFM and Novel Organic Gelation Behavior. *Macromolecules* **2005**, *38*, 334–344.

(4) Welch, P. M.; Welch, C. F. The Effects of Crowding in Dendronized Polymers. *Nano Lett.* **2006**, *6*, 1922−1927.
(5) Schlüter, A. D.; Rabe, J. P. Dendronized Polymers: Synthesis, Characterization, Assembly at Interfaces, and Manipulation. *Angew. Chem., Int. Ed. Engl.* **2000**, *39*, 864−883.
(6) Guo, Y.; van Beek, J. D.; Zhang, B.; Colussi, M.; Walde, P.; Zhang, A.; Kröger, M.; Halperin, A.; Schlüter, A. D. Tuning Polymer Thickness: Synthesis and Scaling Theory of Homologous Series of Dendronized Polymers. *J. Am. Chem. Soc.* **2009**, *131*, 11841−11854.
(7) Lee, C. C.; Yoshida, M.; Fréchet, J. M. J.; Dy, E. E.; Szoka, F. C. In Vitro and in Vivo Evaluation of Hydrophilic Dendronized Linear Polymers. *Bioconjugate Chem.* **2005**, *16*, 535−541.
(8) Gillies, E. R.; Fréchet, J. M. J. Dendrimers and Dendritic Polymers in Drug Delivery. *Drug Discovery Today* **2005**, *10*, 35−43.
(9) Liang, C. O.; Helms, B.; Hawker, C. J.; Fréchet, J. M. J. Dendronized Cyclocopolymers with a Radial Gradient of Polarity and Their Use to Catalyze a Difficult Esterification. *Chem. Commun.* **2003**, *20*, 2524−2525.
(10) Deng, G. J.; Yi, B.; Huang, Y. Y.; Tang, W. J.; He, Y. M.; Fan, Q. H. Dendronized Poly(Ru-BINAP) Complexes: Highly Effective and Easily Recyclable Catalysts For Asymmetric Hydrogenation. *Adv. Synth. Catal.* **2004**, *346*, 1440−1444.
(11) Fornera, S.; Balmer, T. E.; Zhang, B.; Schlüter, A. D.; Walde, P. Immobilization of Peroxidase on SiO_2 Surfaces with the Help of a Dendronized Polymer and the Avidin-Biotin System. *Macromol. Biosci.* **2011**, *11*, 1052−1067.
(12) Grotzky, A.; Nauser, T.; Erdogan, H.; Schlüter, A. D.; Walde, P. A Fluorescently Labeled Dendronized Polymer-Enzyme Conjugate Carrying Multiple Copies of Two Different Types of Active Enzymes. *J. Am. Chem. Soc.* **2012**, *134*, 11392−11395.
(13) Rodríguez-Ropero, F.; Canales, M.; Zanuy, D.; Zhang, A.; Schlüter, A. D.; Alemán, C. Helical Dendronized Polymers with Chiral Second-Generation Dendrons: Atomistic View and Driving Forces for Structure Formation. *J. Phys. Chem. B* **2009**, *113*, 14868−14876.
(14) Zhang, A.; Rodríguez-Ropero, F.; Zanuy, D.; Alemán, C.; Meijer, E. W.; Schlüter, A. D. A Rigid, Chiral, Dendronized Polymer with a Thermally Stable, Right-Handed Helical Conformation. *Chem.—Eur. J.* **2008**, *14*, 6924−6934.
(15) Ding, Y.; Öttinger, H. C.; Schlüter, A. D.; Kröger, M. From Atomistic Simulation to the Dynamics, Structure and Helical Network Formation of Dendronized Polymers: The Janus Chain Model. *J. Chem. Phys.* **2007**, *127*, 0943904-7.
(16) Leung, K. C. F.; Mendes, P. M.; Magonov, S. N.; Northrop, B. H.; Kim, S.; Patel, K.; Flood, A. H.; Tseng, H. R.; Stoddart, J. F. Supramolecular Self-Assembly of Dendronized Polymers: Reversible Control of the Polymer Architectures through Acid-Base Reactions. *J. Am. Chem. Soc.* **2006**, *128*, 10707−10715.
(17) Stocker, W.; Karakaya, B.; Schurman, B. L.; Rabe, J. P.; Schlüter, A. D. Ordered Dendritic Nanorods with a Poly(para-phenylene) (PPP) Backbone. *J. Am. Chem. Soc.* **1998**, *120*, 7691−7695.
(18) Paulo, P. M. R.; Canongia-Lopes, J. N.; Costa, S. M. B. Molecular Dynamics Simulations of Charged Dendrimers: Low-to-Intermediate Half-Generation PAMAMs. *J. Phys. Chem. B* **2007**, *111*, 10651−10664.
(19) Bertran, O.; Zhang, B.; Schlüter, A. D.; Halperin, A.; Kröger, M.; Alemán, C. Computer Simulations of Dendronized Polymers: Organization and Characterization at the Atomistic Level. *RSC Adv.* **2013**, *3*, 126−140.
(20) Zhang, B.; Wepf, R.; Kröger, M.; Halperin, A.; Schlüter, A. D. Height and Width of Adsorbed Dendronized Polymers: Electron and Atomic Force Microscopy of Homologous Series. *Macromolecules* **2011**, *44*, 6785−6792.
(21) Zhang, B.; Wepf, R.; Fischer, K.; Schmidt, M.; Besse, S.; Lindner, P.; King, B. T.; Sigel, R.; Schurtenberger, P.; Talmon, Y.; et al. The Largest Synthetic Structure with Molecular Precision: Towards a Molecular Object. *Angew. Chem., Int. Ed.* **2011**, *50*, 763−766.
(22) Phillips, J. C.; Braun, R.; Wang, W.; Gumbart, J.; Tajkhorshid, E.; Villa, E.; Chipot, C.; Skeel, R. D.; Kale, L.; Schulten, K. Scalable Molecular Dynamics with NAMD. *J. Comput. Chem.* **2005**, *26*, 1781−1802.
(23) Cornell, W. D.; Cieplak, P.; Bayly, C. I.; Gould, I. R.; Merz, K. M.; Ferguson, D. M.; Spellmeyer, D. C.; Fox, T.; Caldwell, J. W.; Kollman, P. A. A Second Generation Force Field for the Simulation of Proteins, Nucleic Acids, and Organic Molecules. *J. Am. Chem. Soc.* **1995**, *117*, 5179−5197.
(24) Wang, J.; Wolf, R. M.; Caldwell, J. W.; Case, D. A. Development and Testing of a General Amber Force Field. *J. Comput. Chem.* **2004**, *15*, 1157−1174.
(25) Cieplak, P.; Cornell, W.; Bayly, C. I.; Kollman, P. A. Application of the Multimolecule and Multiconformational RESP Methodology to Biopolymers: Charge Derivation for DNA, RNA, and Proteins. *J. Comput. Chem.* **1995**, *16*, 1357−1377.
(26) Ryckaert, J. P.; Ciccotti, G.; Berendsen, H. J. C. Numerical Integration of the Cartesian Equations of Motion of a System with Constraints: Molecular Dynamics of n-Alkanes. *J. Comput. Phys.* **1977**, *23*, 327−341.
(27) Jorgensen, W. L.; Chandrasekhar, J.; Madura, J. D.; Impey, R. W.; Klein, M. L. Comparison of Simple Potential Functions for Simulating Liquid Water. *J. Chem. Phys.* **1983**, *79*, 926−935.
(28) Darden, T.; York, D.; Pedersen, L. Particle Mesh Ewald: An $N\cdot\log(N)$ Method for Ewald Sums in Large Systems. *J. Chem. Phys.* **1993**, *98*, 10089-4.
(29) Casanovas, J.; Canales, M.; Fabregat, G.; Meneguzzi, A.; Alemán, C. Water Absorbed by Polyaniline Emeraldine Tends to Organize, Forming Nanodrops. *J. Phys. Chem. B* **2012**, *116*, 7342−7350.
(30) Taylor, R. B.; Kennard, O. Hydrogen-Bond Geometry in Organic Crystals. *Acc. Chem. Res.* **1984**, 320−326.